Bauer, K.W., et al., 2021, Pulsed volcanism and rapid oceanic deoxygenation during Oceanic Anoxic Event 1a: Geology, v. 49, https://doi.org/10.1130/G49065.1

Supplemental Material Pulsed volcanism and rapid ocean deoxygenation during OAE1a

[1]Kohen W. Bauer, [2]Cinzia Bottini, [3]Robert Frei, [4]Dan Asael, [4]Noah J. Planavsky, [5]Roger Francois, [1]N. Ryan McKenzie, [3]Elisabetta Erba and [5*]Sean A. Crowe

[1]Department of Earth Science, University of Hong Kong

[2]Department of Earth Sciences, University of Milan

[3]Department of Geosciences and Natural Resource Management, University of Copenhagen

[4]Department of Geology and Geophysics, Yale University

[5]Departments EOAS and M&I UBC
University of British Columbia

*Correspondence; Sean Crowe (sean.crowe@ubc.ca)

SUPPLEMENTARY METHODS

Geological Setting

We worked with samples from the Cismon APTICORE, a reference section for the Barremian-Aptian interval at low latitudes (Bottini et al., 2012; Erba and Larson, 1998; Menegatti et al., 1998). The site was located on the continental margin of the Mesozoic Tethys, on the eastward deepening slope between the Trento Plateau and the Belluno Basin (Bottini et al., 2012). Lithologically the Selli Level (representing OAE1a) is characterized by marlstone alternating with black shales and discrete radiolarian beds (Erba and Larson, 1998). We targeted our Fe-speciation analyses on intervals also studied in (Bottini et al., 2012). DSDP Site 463 was drilled at a water depth of 2525 m in the ancient structural high of the western Mid-Pacific Mountains (21°21.01'N, 174°40.07'E) (Bottini et al., 2012). During the Early Cretaceous, Site 463 was located at a paleo-latitude of ~20°S with a paleo-depth of ~1 km (Roth, 1981). The OAE1a occurs at Site 463 between ~626-615 mbsf, corresponding to ~12 m of tuffaceous limestone (Ando et al., 2002) containing a number of discrete organic-rich horizons with TOC up to 7.5

(wt%) (Erba, 2004; van Breugel et al., 2007). See Figure (S1) for a paleogeographic reconstruction of the early Aptian.

Sediment digestions

Rock samples from both Cismon and DSDP Site 463 drill cores were crushed using an agate mill to avoid metal contamination, and crushed sediment samples were then further milled to fine powders using an agate hand mortar and pestle. Sample splits (200 mg) were totally digested using lithium metaborate fusion (Garbeschonberg, 1993). We utilized a sample to LiO_2 flux ratio of 1:1. Sediments splits of 500 mg were also weighed into 50 mL centrifuge tubes and subjected to a 0.5 N HCl leach for 1 hr. Elemental abundances and Cr isotope compositions were determined in both the bulk fusion digestions and the 0.5 N HCl leaches. The Fe-speciation data was previously produced by Bauer et al. ((2019)p). For Fe-speciation, sample splits of 500 mg of sediment were subjected to the Fe-speciation sequential extraction scheme (Poulton and Canfield, 2005). Bauer et al. ((2019)p) also performed a revised extraction scheme that included an organic matter leach. All data is tabulated in Table S1.

Trace element concentrations in our leachates were measured by quadrupole inductively coupled plasma mass spectroscopy (Q-ICP-MS) at the University of Hong Kong, while major elemental concentrations in our leachates were determined by inductively coupled optical emission mass spectroscopy (ICP-OES) at the University of British Columbia. For our Q-ICP-MS measurements, precision on Cr was <1% RSD and our limit of detection in solution was 0.03 μg L^{-1}, or roughly 19 μg kg^{-1} Cr based on our dilutions. For our Q-ICP-MS measurements precision for all REEs was ~1.0% RSD and our limit of detection in solution was typically ~1 ng L^{-1}, or roughly 0.2 μg kg^{-1} based on our dilutions. For Al analysis via ICP-OES, precision was 0.4% RSD and our limit of detection in solution was 100 μg L^{-1}, or roughly 27 μg g^{-1} based on our dilutions. For Mn analysis via ICP-OES, precision was 0.3% RSD and our limit of detection in solution was 7 μg L^{-1}, or roughly 2 μg g^{-1} based on our dilutions. Our fusion digestions dissolved ~100%, 97% and 100% of the Cr in the BHVO-2, MESS-3, and PACS-2 international reference standards, respectively. Our fusion digestions dissolved 100%, 98%, and 100%

of Ce in the BHVO-2, MESS-3, and PACS-2 international reference standards, respectively, and similar results were obtained for all the REEs.

Cr purification and isotope ratio determination

Chromium isotope ratios in the Cismon fusions were determined on a Multi-Collector Inductively-Coupled Plasma Mass Spectrometer (MC-ICP-MS) at the Yale Metal Geochemistry Center using a double-spike correction for isotope fractionation during column chemistry and instrumental mass bias. The spike was added to acid splits after the digestion procedure. Although isotope effects due to leaching procedures have not been tested directly, we do not expect any measurable isotope fractionation during acid digestions of Cr, even at higher acid molarity (see Crowe et al. (2013) and Reinhard et al. (2013)). We note that previous studies on Fe isotope ratios in rocks and sediments have also shown that there appears to be no isotope effect during proton-promoted acid leaching of Fe oxides, which is in contrast to ligand promoted dissolution (Wiederhold et al., 2006). We used three separate column separations (Reinhard et al., 2014; Schoenberg et al., 2008) to ensure complete removal of Fe, Ti, and V during chemical purification. Initially, a split of the 6 N HCl sample solution was spiked, evaporated to dryness, and the residues brought up in 1 N HCl. The amounts of ^{50}Cr-^{54}Cr double-spike (^{50}Cr/^{52}Cr = 462.917, ^{53}Cr/^{52}Cr = 0.580, ^{54}Cr/^{52}Cr = 354.450, calibrated in the Department of Geology, University of Illinois at Urbana-Champagne and added as Cr(III)), were adjusted so that the spike/sample ratio (i.e., $(^{54}Cr)_{spk}/(^{52}Cr)_{smp}$) was 0.5. Prior to the first column step (AG1-X8 anionic resin, 100-200 mesh), Cr(III) was oxidized to Cr(VI) using potassium peroxidisulfate (heating the samples for 2 h at 110 °C). The AG1-X8 resin was cleaned with mQ water, 3 N HNO_3 and 6 N HCl. The matrix was eluted with 24 ml of 0.2 N HCl and 4 ml 2 N HCl, with Cr subsequently reduced with 5% H_2O_2 and eluted with 5 ml of 2 N HNO_3. The second step removes traces of Fe that may remain after the first elution. Microcolumns were filled with 0.2 ml AG1-X8 resin. The columns were cleaned using mQ water and 3 N HNO_3, and samples were loaded and collected with 1.2 ml of 6 N HCl. Traces of Ti are often left after the first two column steps. Therefore, as the last step, a cation resin AG50W-X8 (200-400 mesh) was used to ensure complete Ti and Cr separation. The resin was cleaned with mQ water, 3 N HNO_3 and 6 N HCl, followed by

sample loading in 3 ml of 0.5 N HNO_3 and by matrix elution with 1 ml of 0.5 N HNO_3, 2 ml of 0.5 N HF and 6 ml of 1 N HCl. Cr was collected after loading with 4 ml of 0.5 N HNO_3 and after elution with 5 ml of 1.8 N HCl.

Chromium isotopes were measured on a NeptunePlus (Thermo-Finnigan) MC-ICP-MS using a modified version of the analytical protocol of Schoenberg et al. (2008). Samples were run in high-resolution mode to resolve polyatomic interferences such as $^{40}Ar^{12}C^{+}$, $^{40}Ar^{14}N^{+}$ and $^{40}Ar^{16}O^{+}$. Although our chemical procedure results in nearly complete removal of Fe, Ti and V, these elements were monitored by measuring ^{56}Fe, ^{49}Ti and ^{51}V, and samples were corrected for potential interferences of ^{54}Fe on ^{54}Cr, as well as ^{50}Ti and ^{50}V on ^{50}Cr. Samples at a concentration of ~100 ng/g were introduced into the plasma with a PFA μFlow nebulizer (~50 μL/min) coupled with an Apex IR (Elemental Scientific) without additional N_2 gas or membrane desolvation. With a standard sample cone and X skimmer cone, the sensitivity obtained was ~3×10^{-10} A ^{52}Cr on 100 ng/g solution. All ion beams were measured on faraday detectors. The double-spike data reduction model is based on the iterative method described by Siebert et al. (2001). A spiked Cr isotope standard NIST SRM 979 was measured bracketing every three natural samples to ensure machine stability. Chromium isotope ratios are reported relative to bracketing standards using conventional delta notation ($\delta^{53}Cr = [(^{53}Cr/^{52}Cr)_{sample}/(^{53}Cr/^{52}Cr)_{NIST\text{-}979} - 1] \times 1000‰$).

External precision is reported as two sigma (2σ) uncertainty, calculated based on duplicate analysis of geological reference materials (GRMs) processed through ion-exchange chromatography columns along with samples (BHVO-2 was systematically processed with each batch of 24 samples). The $\delta^{53}Cr$ value for BHVO-2 is -0.12 ± 0.07‰ (n = 3), which is similar to published values in the literature for BHVO-1 (geostandard collected at the same location as BHVO-2) (Schoenberg et al., 2008). Sample duplicates, including column procedure duplicates, digested duplicates, and replicate measurements on the MC-ICP-MS revealed a 2σ uncertainty similar to that determined for GRMs, i.e. ≤ 0.09‰ and an average duplicate offset of 0.043‰. Measurement precision is calculated via replicate measurements of the isotopic standard NIST SRM 979 during each analytical session, and 2σ values are better than 0.04‰. In addition, a two-standard deviation of the mean (2se) was systematically calculated using the 50 cycles of

measurement obtained for each sample during MC-ICP-MS analysis, and was generally 0.04-0.06‰ on the delta values. This precision and accuracy are comparable to long term means at the Yale Metal Geochemistry Center.

Chromium separations of the DSDP Site 463 fusions, DSDP Site 463 0.5 N HCl digests, and Cismon 0.5 N HCl digests were processed in the labs of University of Copenhagen and chromium isotope ratios were determined on a Thermal Ionization Mass Spectrometer (IsotopX Phoenix) at the Danish Center for Isotope Geology, University of Copenhagen, using a double-spike correction for isotope fractionation during column chemistry and instrumental mass bias. An adequate amount of ^{50}Cr-^{54}Cr double spike was added to the sample digests and dried down on a hotplate at 80 °C. To ensure spike – sample homogenization, the spiked samples were re-dissolved in *aqua regia* and dried down again. The final residues were then ready for ion chromatographic elution. Cr was separated from the sample matrix using a three-step chromatographic elution procedure: The first step served the removal of Fe from the samples. The dried down samples were dissolved in 1 ml 6 N double distilled HCl. Anion exchange columns were loaded with ~2 ml of pre-cleaned Dowex AG 1×8 anion resin (100–200 mesh) and conditioned with 6 N HCl, before passing over the dissolved samples. To ensure a high Cr yield the columns were further washed with 5 ml of 6 N double distilled HCl. The collected solutions were dried down on a hot plate at 130 °C. In the second step, V and Ti were removed from the samples. For that the dried down residues were dissolved in 20 ml of pure 18 MΩ MilliQ water (MQ) and acidified with 0.5 ml 1 N HCl. Further, 0.5 ml of a freshly prepared 1 N ammonium persulfate ($(NH_4)_2S_2O_8$) solution was added to the samples to oxidize Cr(III) to Cr (VI) (Ball and Bassett, 2000). A full oxidation was ensured by boiling the samples in closed Teflon beakers on a hot plate at 130 °C for 1 h. After cooling down, the samples were passed over a second set of anion exchange columns (BioRad) loaded with ~2 ml of pre-cleaned Dowex AG 1×8 anion resin and pre-conditioned with 0.1 N HCl (100–200 mesh). Subsequently, 10 ml of 0.2 N HCl, 2 ml of 2 N HCl and 5 ml of MQ, were passed over the columns to wash the matrix. Finally, Cr was reduced and collected using 6 ml 2 N HNO_3 doped with a few drops of 5% H_2O_2 and dried down overnight. In the third and final step, Cr was separated from major matrix elements such as Ca, Mg, Mn and Al as well as residual Fe. Cation exchange columns were loaded with ~2 ml of pre-cleaned

Dowex AG50W-X8 cation resin (200–400 mesh) and conditioned with 0.5 N HCl. The dried down samples were dissolved in 2.4 ml 0.5 N double distilled HCl and passed over the prepared columns. To better the Cr yield an additional 8 ml 0.5 N double distilled HCl were passed over the columns and collected. The final solutions were dried down on a hot plate at 130 °C and the resulting Cr precipitates were ready for Cr isotopic analyses.

An IsotopX Phoenix thermal ionization mass spectrometer equipped with eight Faraday collectors was used for all the Cr isotope measurements. This system allows the simultaneous collection of the $^{50}Cr+$, $^{52}Cr+$, $^{53}Cr+$, $^{54}Cr+$ and interfering $^{49}Ti+$, $^{51}V+$, and $^{56}Fe+$ masses. A loading mixture of 1 µl H_3PO_4, 0.5 µl H_3BO_3 and 2.5 µl silicic acid (Gerstenberger and Haase, 1997) was used to load the final Cr precipitates onto outgassed Re-filaments. The samples were analyzed at temperatures between 1050 °C to 1250 °C and ^{52}Cr beam intensities of 0.5 V. A minimum of five runs was conducted for each sample, with one run consisting of 120 cycles, which was grouped into 12 blocks of 10 cycles. The Cr isotopic composition ($\delta^{53}Cr$) of the samples is given in ‰ as the average of the runs relative to the international standard NIST SRM 979 ($\delta^{53}Cr$ (‰)=(($^{53}Cr/^{52}Cr$sample) / ($^{53}Cr/^{52}Cr$NIST SRM 979)−1)×1000) and the analyses error as the double standard deviation (± 2σ) of the runs. Internal analyses errors were as high as 0.12‰ (2σ), but most commonly the error was below the external standard reproducibility error (± 0.07‰; 2σ). Procedural Cr blanks were typically between 2 and 4 ng of Cr, an amount that is negligible considering that a total of 250 ng of Cr was processed in the samples.

Cr isotope mass balance

We corrected both the bulk ($\delta^{53}Cr_{Bulk}$) and 0.5 N HCl leachable $\delta^{53}Cr$ ($\delta^{53}Cr_{HCl}$) values for the detrital Cr contribution by calculating their model authigenic composition values using the following equation (see Data Repository);

$$\delta^{53}Cr_{Authigenic} = \left([\delta^{53}Cr \ - \delta^{53}Cr_{Detrital} \cdot (1 - f_{Authigenic})\right] / f_{Authigenic} \quad (1)$$

where $\delta^{53}Cr_{Detrital}$ was set to the composition of the igneous silicate Earth (ISE) (-0.121‰, Schoenberg et al. (2008)) and $f_{Authigenic}$ was calculated using the Cr/Al and Cr/Sc-ratios of

the Post Achaean Australian Shale (PAAS) (McLennan, 2001). The assumption here is that the entirety of the Al and Sc in the sediment is of detrital origin. In the Cismon sediments, 0.5 N HCl leached on average ~2% of the total Al, implying limited detrital Cr contribution to this leachate. Even with a small detrital contribution, $\delta^{53}Cr_{HCl}$ values become heavier once accounting for detrital Cr contained in this leachate (Table S1). In the DSDP Site 463 sediments, 0.5 N HCl leached on average ~ 3% of the total Al, again implying limited detrital Cr contribution to this leachate. However, because $\delta^{53}Cr_{HCl}$ values are already close to the ISE composition, correcting for detrital Cr contained in this leachate has a minimal effect (Table S1). In two samples in DSDP Site 463, $[Cr]_{Bulk}$ contained negligible amounts of authigenic Cr (<5%), and thus the authigenic Cr correction is associated with too great an uncertainty. For these data points with the authigenic Cr (Al-corrected) (<10%) uncorrected $\delta^{53}Cr_{Bulk}$ values are plotted in the figures (Table S1). An obvious area for future research will be to further identify additional sedimentary carrier phases of authigenic Cr and their isotopic compositions.

REE normalizations

All REE abundances in this study were normalized to the PAAS (McLennan, 2001). The Ce anomaly (Ce/Ce*) was defined following Tostevin et al. (2016) and Lawrence et al. (2006);

$$\frac{Ce}{Ce^*} = \frac{Ce_{SN}}{((Pr_{SN})^2/Nd_{SN})} \qquad (2)$$

where the subscript SN refers to an element that has been normalized to the PAAS composition. The Eu anomaly (Eu/Eu*) was defined following (Tostevin et al., 2016);

$$\frac{Eu}{Eu^*} = \frac{2*Eu_{SN}}{(Sm_{SN}+Gd_{SN})} \qquad (3)$$

where the subscript SN refers to an element that has been normalized to the PAAS composition. We also calculated (Eu/Eu*) after (Olivarez and Owen, 1991);

$$\frac{Eu}{Eu^*} = log_{10}(\frac{2}{3} * Sm_{SN} + \frac{1}{3} * Tb) \qquad (4)$$

where the subscript SN refers to an element that has been normalized to the PAAS composition. The Pr anomaly (Pr/Pr*) was defined following (Bau and Dulski, 1996);

$$\frac{Pr}{Pr^*} = \frac{2*Pr_{SN}}{(Ce_{SN}+Nd_{SN})} \qquad (5)$$

where the subscript SN refers to an element that has been normalized to the PAAS composition. The bell-shape index (BSI) was defined as being equal to the weighted ratio between shale-normalized middle REE (mREE), and shale-normalized light (lREE) and heavy REE (hREE), excluding Ce;

$$BSI = \frac{2*mREE}{(lREE+hREE)} \qquad (6)$$

$$lREE = \frac{(La_{SN}+Pr_{SN}+Nd_{SN})}{3} \qquad (7)$$

$$mREE = \frac{(Sm_{SN}+Eu_{SN}+Gd_{SN}+Tb_{SN}+Dy_{SN})}{5} \qquad (8)$$

$$hREE = \frac{(Ho_{SN}+Er_{SN}+Tm_{SN}+Yb_{SN}+Lu_{SN})}{5} \qquad (9)$$

Fidelity of REE patterns

Distortion of the primary REE signals, known as pattern arching, can occur during sediment diagenesis, which would impair their use as palaeoenvironmental proxies. Thus, we verified the degree to which the observed REE patterns may have been subject to diagenetic overprinting and/or silicilastic contamination using a number of detailed tests. BSI values are used to assess post-depositional REE enrichment from phosphates or oxide phases (Bau and Dulski, 1996). The average BSI in Cismon core is BSI_{Bulk} = 1.3 and $BSI_{0.5\ N\ HCl}$ = 1.6, whereas in the DSDP Site 463 sediments average values are BSI_{Bulk} = 1.4 and $BSI_{0.5\ N\ HCl}$ = 2.0 (Table S1). These BSI values are low and indicative of negligible post-depositional REE enrichment from phosphates or oxide phases (Bau and Dulski, 1996) (Fig. S3). Ce anomalies can also be artificially created by La enrichment, creating a false diagnosis of varying redox conditions. To assess this potential effect, we

constructed a La anomaly diagram (Pr/Pr* vs. Ce/Ce*), which is used to trace potential La anomalies generating false Ce anomalies. The La anomaly diagram (Fig. S2) shows that the Ce/Ce* in the Cismon sediments is not due to anomalous La enrichment and may therefore be used to trace seawater redox conditions. Furthermore, a lack of positive correlation between Ce/Ce* and Eu/Eu* at both sites implies the anomalies are primary (Shields and Stille, 2001) (Fig. S2). However, a few samples from DSDP Site 463 do plot in field (IIa), which would signify a positive La anomaly causing an apparent negative Ce anomaly. Therefore, we used additional means to verify that the REE signatures were not severely affected by diagenetic processes at both sites, which we detail below.

Examining the concentration and correlation of Sc with REE abundances can be used to monitor siliciclastic contaminations because silicate minerals have much higher REE, and Sc contents than other sedimentary phases, causing deviations in REE distributions (Bodin et al., 2013). In the Cismon sediments, there is no positive correlation between Sc and Eu/Eu* and only a weak positive correlation between Sc and Pr/Pr*, and Ce/Ce* ($r^2 = 0.30$ and $r^2 = 0.51$, respectively) (Fig. S3). Additionally, there is no positive correlation between BSI and Pr/Pr*, Ce/Ce* or Eu/Eu*. In the DSDP Site 463 sediments, there is only weak positive correlations between Sc and Pr/Pr*, Ce/Ce*, and Eu/Eu* ($r^2 = 0.40$, r2 =0.40, and $r^2 = 0.45$, respectively) and no positive correlations between BSI and Pr/Pr*, Ce/Ce* or Eu/Eu* (Fig. S3). Notably, in no case do both the bulk and 0.5 N HCl extractable pools display similarly positive correlations between these variables (Fig. S3). These results strongly indicate that the REE signals in either the bulk or 0.5 N HCl pools, and in most cases both the bulk and 0.5 N HCl pools in both the Cismon and DSDP Site 463 sediments are indeed primary and are not due to appreciable diagenetic alteration and REE pattern arching, and thus faithfully record seawater signatures. Regardless, because some weak correlations between the Sc and Al content and REE anomalies do exist, one cannot completely exclude a small amount of siliciclastic contamination (Fig. S4). To further address this issue we compared Ce/Ce* ratio with the Dy_{SN}/Sm_{SN} ratios as an indicator of arching in the REE patterns (Shields and Stille, 2001). Any significant co-variation of both parameters would signify Ce/Ce* primarily driven by arching of the REE pattern. In both the bulk and 0.5 N HCl sediment pools at the Cismon and DSDP sites, there are no positive correlations between these two

values ($r^2 < 0.35$) (Table S1). Thus, through multiple means we verified that the REE patterns in both the bulk and 0.5 N HCl sediments pools at Cismon and DSDP Site 463 sites are primary and can be applied effectively as palaeoenvironmental indicators.

Figures and Tables

Table S1. Cismon and DSDP Site 463 sediment elemental concentrations and Cr isotope compositions.

Separate .xls file attached.

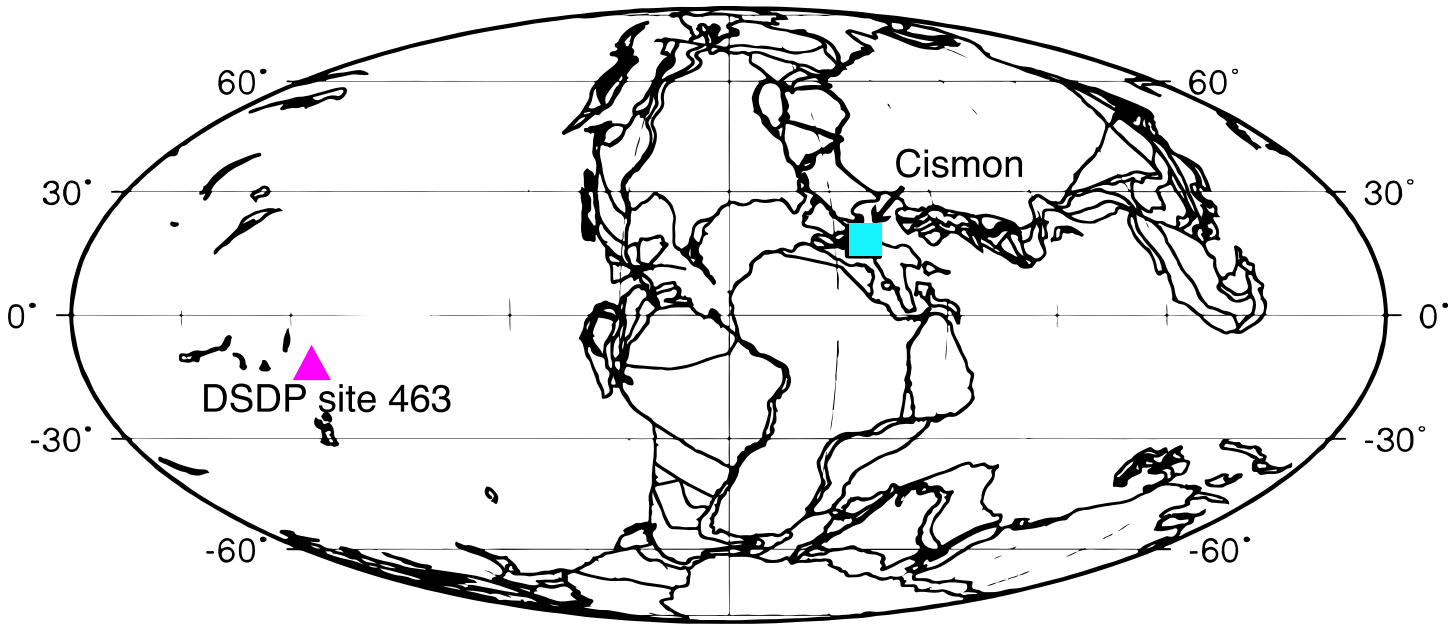

Fig. S1. Paleogeographic reconstruction of the early Aptian (~120 Ma), redrafted after (Gomes et al., 2016).

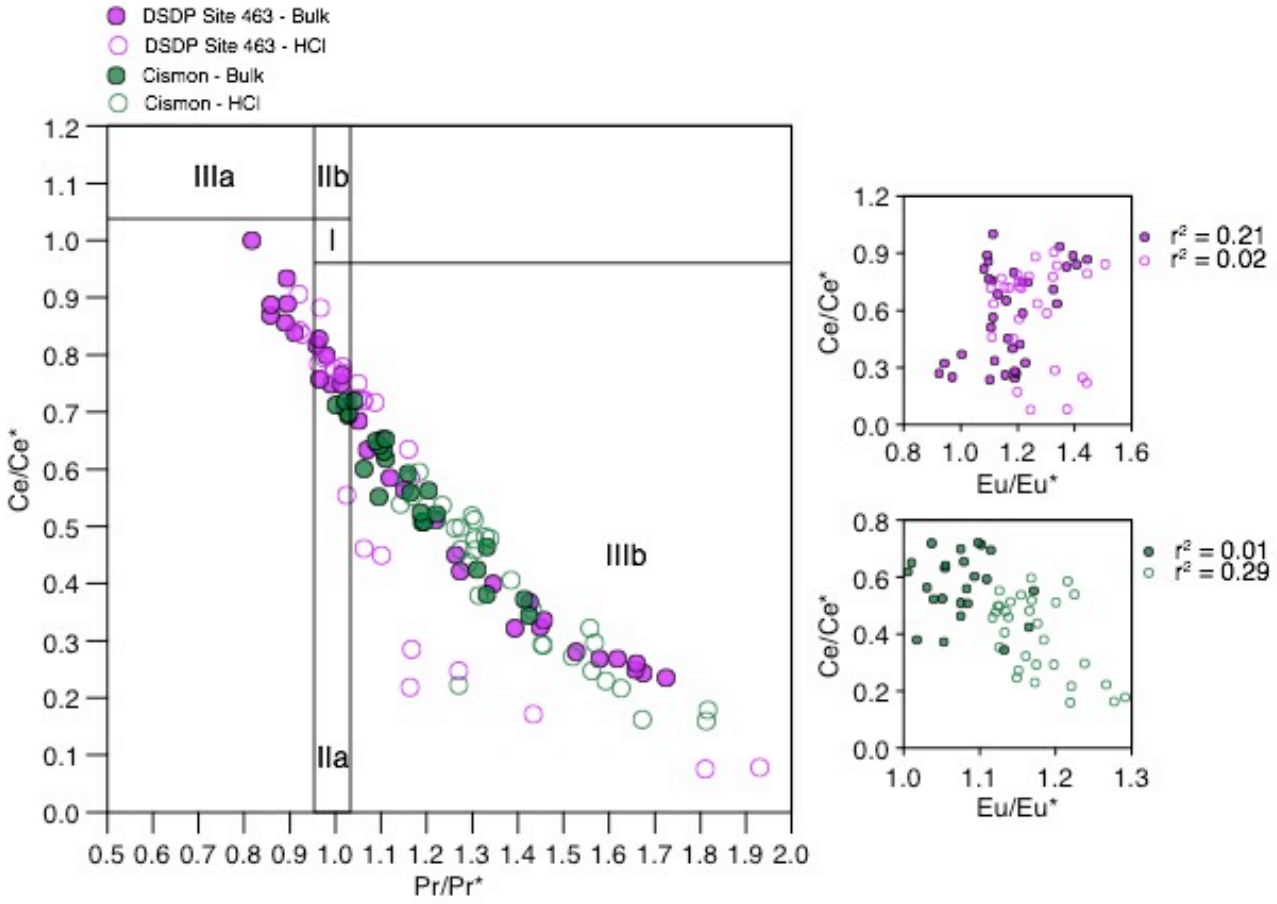

Fig. S2. La anomaly diagram and Ce/Ce* vs. Eu/Eu* cross-plots. Ce/Ce* vs. Pr/Pr* after (Bau and Dulski, 1996). Field I: no anomaly; Field IIa: positive La anomaly causes apparent negative Ce anomaly; Field IIb: negative La anomaly causes apparent positive Ce anomaly; Field IIIa: real positive Ce anomaly; Field IIIb: real negative Ce anomaly, in which La enrichment may still lead to overestimated, and MREE arching to underestimated Ce anomalies. For the Ce/Ce* vs. Eu/Eu* cross-plots we have conducted linear regressions for which the r^2 values are displayed to the right of the panels. We do not display the lines for figure clarity.

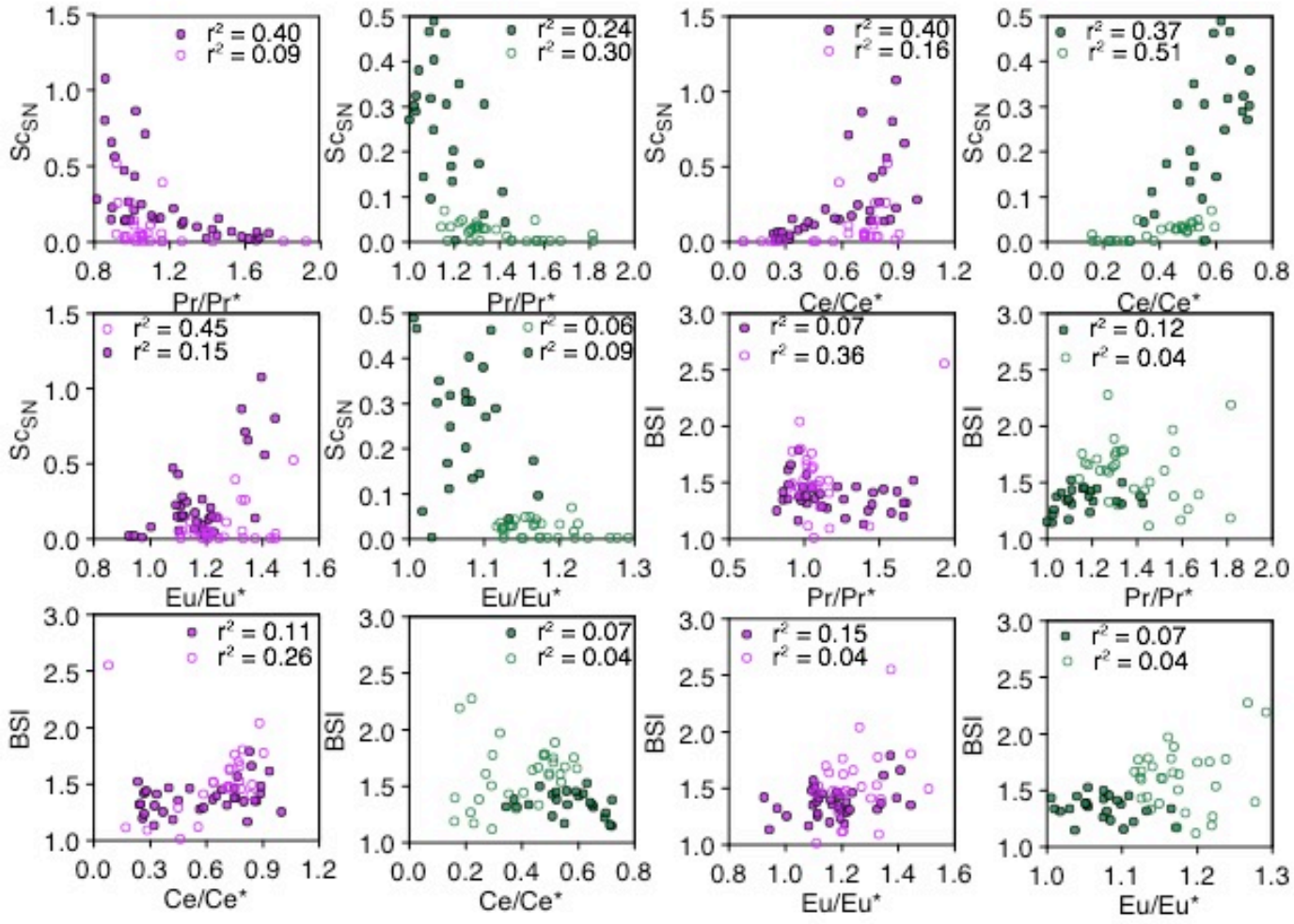

Fig. S3. REE and cross plots. Magenta data corresponds to DSDP Site 463 bulk (closed circles) and 0.5 N HCl leaches (open circles). Green data corresponds to Cismon bulk (closed circles) and 0.5 N HCl leaches (open circles). We have conducted linear regressions but do not display the line for figure clarity. The r^2 value on each regression is displayed in each panel.

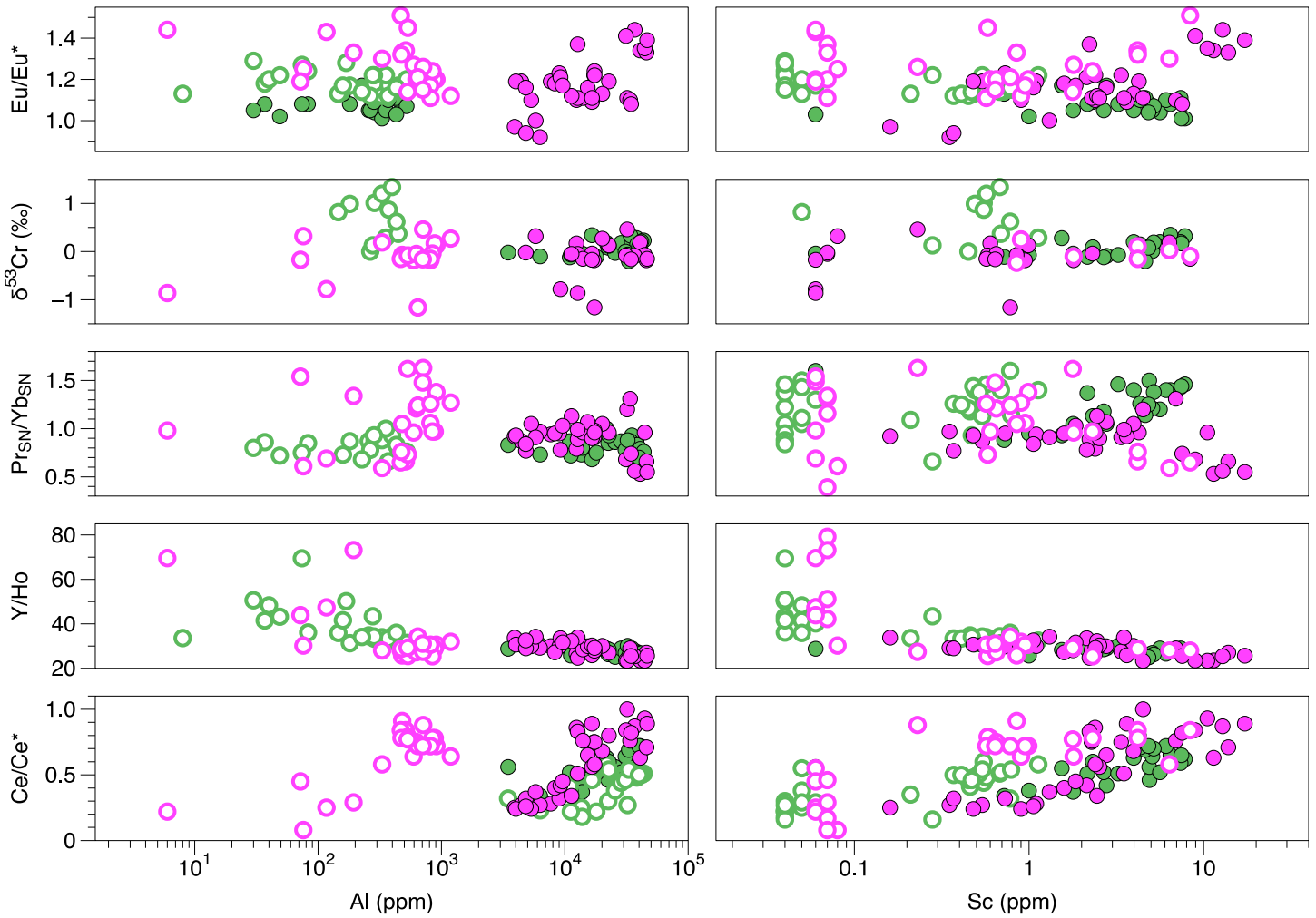

Fig. S4. REE and $\delta^{53}Cr$ cross plots. Magenta data corresponds to DSDP Site 463 bulk (closed circles) and 0.5 N HCl leaches (open circles). Green data corresponds to Cismon bulk (closed circles) and 0.5 N HCl leaches (open circles). Variability in the REE + Y and $\delta^{53}Cr$ patterns do not correspond with degrees of detrital sediment contribution.

References

Ando, A., Kakegawa, T., Takashima, R., and Saito, T., 2002, New perspective on Aptian carbon isotope stratigraphy: Data from delta C-13 records of terrestrial organic matter: Geology, v. 30, no. 3, p. 227-230.

Ball, J. W., and Bassett, R. L., 2000, Ion exchange separation of chromium from natural water matrix for stable isotope mass spectrometric analysis: Chemical Geology, v. 168, no. 1-2, p. 123-134.

Bau, M., and Dulski, P., 1996, Distribution of yttrium and rare-earth elements in the Penge and Kuruman iron-formations, Transvaal Supergroup, South Africa: Precambrian Research, v. 79, no. 1-2, p. 37-55.

Bauer, K., Bottini, C., Katsev, S., Jellinek, M., Francois, R., Erba, E., and Crowe, S., (2019)p, Ferruginous oceans during OAE1a and the collapse of the seawater sulphate reservoir.

Bodin, S., Godet, A., Westermann, S., and Follmi, K. B., 2013, Secular change in northwestern Tethyan water-mass oxygenation during the late Hauterivian-early Aptian: Earth and Planetary Science Letters, v. 374, p. 121-131.

Bottini, C., Cohen, A. S., Erba, E., Jenkyns, H. C., and Coe, A. L., 2012, Osmium-isotope evidence for volcanism, weathering, and ocean mixing during the early Aptian OAE 1a: Geology, v. 40, no. 7, p. 583-586.

Crowe, S. A., Dossing, L. N., Beukes, N. J., Bau, M., Kruger, S. J., Frei, R., and Canfield, D. E., 2013, Atmospheric oxygenation three billion years ago: Nature, v. 501, no. 7468, p. 535-+.

Erba, E., 2004, Calcareous nannofossils and Mesozoic oceanic anoxic events: Marine Micropaleontology, v. 52, no. 1-4, p. 85-106.

Erba, E., and Larson, R. L., 1998, The Cismon APTICORE (Southern Alps, Italy): A "reference section" for the Lower Cretaceous at low latitudes: Rivista Italiana Di Paleontologia E Stratigrafia, v. 104, no. 2, p. 181-191.

Gerstenberger, H., and Haase, G., 1997, A highly effective emitter substance for mass spectrometric Pb isotope ratio determinations: Chemical Geology, v. 136, no. 3-4, p. 309-312.

Gomes, M. L., Hurtgen, M. T., and Sageman, B. B., 2016, Biogeochemical sulfur cycling during Cretaceous oceanic anoxic events: A comparison of OAE1a and OAE2: Paleoceanography, v. 31, no. 2, p. 233-251.

Lawrence, M. G., Greig, A., Collerson, K. D., and Kamber, B. S., 2006, Rare earth element and yttrium variability in South East Queensland waterways: Aquatic Geochemistry, v. 12, no. 1, p. 39-72.

McLennan, S. M., 2001, Relationships between the trace element composition of sedimentary rocks and upper continental crust: Geochemistry Geophysics Geosystems, v. 2, p. art. no.-2000GC000109.

Menegatti, A. P., Weissert, H., Brown, R. S., Tyson, R. V., Farrimond, P., Strasser, A., and Caron, M., 1998, High-resolution delta C-13 stratigraphy through the early Aptian "Livello Selli" of the Alpine Tethys: Paleoceanography, v. 13, no. 5.

Olivarez, A. M., and Owen, R. M., 1991, The europium anomaly of seawater: implications for fluvial versus hydrothermal REE inputs to the oceans: Chemical Geology, v. 92, no. 4, p. 317-328.
Poulton, S. W., and Canfield, D. E., 2005, Development of a sequential extraction procedure for iron: implications for iron partitioning in continentally derived particulates: Chemical Geology, v. 214, no. 3-4, p. 209-221.
Reinhard, C. T., Planavsky, N. J., Robbins, L. J., Partin, C. A., Gill, B. C., Lalonde, S. V., Bekker, A., Konhauser, K. O., and Lyons, T. W., 2013, Proterozoic ocean redox and biogeochemical stasis: Proceedings of the National Academy of Sciences of the United States of America, v. 110, no. 14, p. 5357-5362.
Reinhard, C. T., Planavsky, N. J., Wang, X., Fischer, W. W., Johnson, T. M., and Lyons, T. W., 2014, The isotopic composition of authigenic chromium in anoxic marine sediments: A case study from the Cariaco Basin: Earth and Planetary Science Letters, v. 407, p. 9-18.
Roth, P. H., 1981, Mid-Cretaceous nannoplankton from the central Pacific implications for palaeoceanography: Initial Reports of the Deep Sea Drilling Project, v. 62, p. 471-489.
Schoenberg, R., Zink, S., Staubwasser, M., and von Blanckenburg, F., 2008, The stable Cr isotope inventory of solid Earth reservoirs determined by double spike MC-ICP-MS: Chemical Geology, v. 249, no. 3-4, p. 294-306.
Shields, G., and Stille, P., 2001, Diagenetic constraints on the use of cerium anomalies as palaeoseawater redox proxies: an isotopic and REE study of Cambrian phosphorites: Chemical Geology, v. 175, no. 1-2, p. 29-48.
Siebert, C., Nagler, T. F., and Kramers, J. D., 2001, Determination of molybdenum isotope fractionation by double-spike multicollector inductively coupled plasma mass spectrometry: Geochemistry Geophysics Geosystems, v. 2, p. 1032.
Tostevin, R., Shields, G. A., Tarbuck, G. M., He, T., Clarkson, M. O., and Wood, R. A., 2016, Effective use of cerium anomalies as a redox proxy in carbonate-dominated marine settings: Chemical Geology, v. 438, p. 146-162.
van Breugel, Y., Schouten, S., Tsikos, H., Erba, E., Price, G. D., and Damste, J. S. S., 2007, Synchronous negative carbon isotope shifts in marine and terrestrial biomarkers at the onset of the early Aptian oceanic anoxic event 1a: Evidence for the release of C-13-depleted carbon into the atmosphere: Paleoceanography, v. 22, no. 1.
Wiederhold, J. G., Kraemer, S. M., Teutsch, N., Borer, P. M., Halliday, A. N., and Kretzschmar, R., 2006, Iron isotope fractionation during proton-promoted, ligand-controlled, and reductive dissolution of goethite: Environmental science & technology, v. 40, no. 12, p. 3787-3793.